### THEMATIC SECTION: 7TH WORLD CONGRESS ON INTEGRATED COMPUTATIONAL MATERIALS ENGINEERING



### **Coupled Thermal Solidification Process Simulation of Sapphire Growth**

R. A. Trasca<sup>1</sup> · M. Sistaninia<sup>1</sup> · G. Reiss<sup>1</sup> · W. Eßl<sup>1</sup> · P. Raninger<sup>1</sup> · S. Lohrasbi<sup>2</sup>

Received: 31 August 2023 / Accepted: 23 October 2023 / Published online: 14 December 2023 © The Minerals, Metals & Materials Society 2023

#### **Abstract**

Thermal distribution during the sapphire growth process determines to a great extent the thermal stresses and dislocation density in sapphire. In this work, thermal and defect simulations of sapphire growth in a simplified single-boule furnace are presented. The heat transfer in the furnace is modeled via ANSYS Fluent® by considering conduction, convection and radiation effects. A dislocation density-based crystal plasticity model is applied for the numerical simulation of dislocation evolution during the crystal growth of sapphire. The physical models are validated by using a temporal series of measurements in the real furnace geometry, which capture the crystal—melt interface position during the technological growth process. The growth rate and the shape of the crystal growth front are analyzed for different side and top heater powers which result in different thermal distributions in the furnace. It is found that the cooling flux at the crucible bottom wall determines to a great extent the growth profile in the first half of the growth stage. Only toward the end of the growth stage, different top and side power distributions induce different growth front shapes. The effect of the convexity of the growth surface on the generation of dislocation defects is investigated by the crystal plasticity model. The results of simulations show that the convexity of the growth surface has a significant effect on the generation of dislocations.

**Keywords** Sapphire growth process · Heat transfer · CFD simulation · Crystal plasticity model · Dislocation density

#### Introduction

Sapphire crystal has been successfully used in recent years as a substrate for electronic high-end applications such as LEDs and  $\mu$ LEDs, which are considered the next-generation devices for high-resolution displays such as television, smartphone, tablet or laptop. While large sapphire crystals (8", 10" and 12" diameter) can be nowadays produced in industrial plants, obtaining high-quality sapphire single crystals is still challenging. Various types of defects such as low angle grain boundary, bubbles and dislocations occur frequently in the sapphire growth applications, and various methods are employed to ensure high-quality products [1, 2]. One characteristic of all methods is the systematic control of the sapphire environmental thermal conditions since these determine the residual stresses and the generation of defects in the sapphire growth process [3].

The main technological methods that are usually employed for the growth of sapphire crystals are the Kyropoulos, Czochralski, vertical Bridgman and heat exchanger method (HEM) [4]. The simulations presented in this paper are validated with measurement data from a HEM growth process. The HEM industrial process of sapphire growth consists of three stages: the melting/seeding phase, the growth phase and the cooling phase. In the melting phase, the sapphire raw material is melted by gradually increasing the heaters power while a sapphire seed is preserved by local cooling at the crucible bottom wall. In the growth stage, the sapphire melt is gradually solidified by slowly decreasing the heater power and manipulating the cooling flux at the sapphire bottom. In the cooling stage, the heaters power is decreased to 0 at specific rates. The aim of any single-crystal growth process is to enhance the quality by minimizing the generation of dislocations, bubble formation and low angle grain boundaries during growth and cooling stages.

Numerical models have been developed for each technological method used to grow sapphire crystals [5–8]. If the furnace geometry has cylindrical symmetry, which is usually



 <sup>⊠</sup> R. A. Trasca Raluca.trasca@mcl.at

Materials Center Leoben Forschung GmbH, Rossegerstr. 12, 8700 Leoben, Austria

<sup>&</sup>lt;sup>2</sup> FAMETEC GmbH, Ebner-Platz 1, 4060 Leonding, Austria

the case for one-boule sapphire growth, a 2D axisymmetric model is employed in simulations. This has the advantage of reducing the computational cost, while capturing the heat transport and flow mechanisms present in furnace atmosphere, insulation and sapphire melt/crystal during the growth process. The main heat transfer mechanisms considered in simulations of the sapphire growth are: thermal radiation at the atmosphere-solid and fluid(melt)-solid exposed surfaces, heat conduction in solid parts, conduction, internal radiation and convection in sapphire melt and conduction and internal radiation in sapphire crystal. The sapphire solidification is modeled in these papers by the enthalpy–porosity approach. A key contribution to the heat transport in sapphire comes from internal radiation, as shown in many studies [8-10]. In sapphire growth by Kyropoulos method, internal radiation increases the heat transfer of both the melt and the crystal, makes temperature distribution uniform, weakens melt convection and reduces stress level in crystal [10]. In the case of the heat exchanger method, it has been found that internal radiation greatly enhances the total heat flux through the crystal, reduces the temperature gradient and thermal stress in the central body of the crystal, but increases the thermal gradients at the sapphire bottom region; therefore, it cannot be neglected in modeling [8, 9].

In the growth stage, the crystal growth rate and the melt-crystal (m-c) interface shape play an essential role in the defect formation. A large growth rate leads to interface breakdown and contamination by impurities or dissolved gas, whereas a large interface convexity promotes the formation of crystal facets with different orientations which can destroy the single-crystal growth or lead to low angle grain boundaries [1]. On the other hand, a small convex shape of the interface can push impurities outwards and prevent nucleation from the crucible walls [11]. The interface convexity is also related to the thermal stresses in sapphire: lower convexity corresponds usually to lower thermal gradient and thermal stresses; therefore in general, a small convex shape of the m-c interface is desirable [12, 13]. Various numerical studies have been performed to optimize the convexity of the m-c interface [7, 8, 13, 14]. The common idea is to minimize the radial to axial heat transfer ratio in sapphire either by optimizing the HEM cooling system geometry or by placing the crucible at the optimum position relative to heaters. However, there is no general recipe for all furnace geometries, and individual solutions are employed in each case. In the present study, we aim to generate different radial to axial thermal gradients in sapphire by using different top and side heater power ratios and to investigate the influence of different setups on the m-c interface shape.

The organization of the paper is as follows. In Section II, a 2D axisymmetric furnace model and the process simulation model are introduced. In the furnace model, the main furnace parts and their material properties are presented. In

the process simulation model, heat transfer mechanisms in different parts of the furnace are discussed with a special focus on the radiative heat transfer. Sapphire melt flow and solidification models are also shortly introduced. In Section III, a PID control loop method for the sapphire seed formation is presented, and the main results of the thermal solidification simulations are discussed. Three cases with different top and side heater power ratios are considered, and a recipe for growth simulations is presented. A qualitative comparison with a sapphire crystal growth measurement is shown to ensure realistic growth rates values. For three cases, the m-c interface shapes during the growth stage are analyzed and compared. Finally, a dislocation density-based crystal plasticity model [15] is applied for the FEM simulation of dislocation evolution during the crystal growth of sapphire. The aim of this simulation is to evaluate the effect of the convexity of the growth surface on the generation of dislocation defects.

### **Model Description**

# Two-Dimensional Axisymmetric Model of the Furnace Geometry

The schematic design of the furnace used in these studies is presented in Fig. 1. This design is a simplification of the original HEM furnace. Here, a 2D axisymmetric geometrical model is used, which is common practice for simulations of

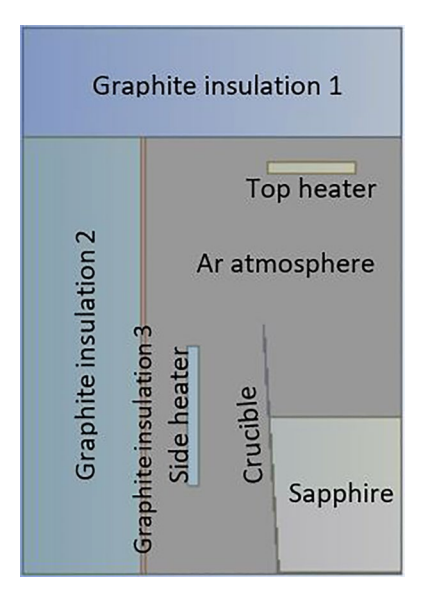


Fig. 1 Schematic picture of the 2D axisymmetric model of the furnace. Due to symmetry, only half of the furnace is used in simulations and shown here. Relevant dimensions: sapphire boule radius=10,75 cm=a; sapphire height=1,5a; crucible height=2,4a; crucible thickness=0,02a; insulation width=a; geometry height=5,5a; and geometry half-width=3,6a



sapphire growth in furnaces with cylindrical symmetry [5, 6, 8]. In the simplified design only the graphite insulation, the inner Ar atmosphere, the top and side heaters and the crucible and the sapphire melt/crystal are considered. The top and side heaters geometries are also simplified so that their volumes correspond to the original top and side heater volumes in the real furnace. The molybdenum crucible is suitable for the growth of an 8" sapphire crystal. Sapphire properties are collected from different references [[5], [16], [4]] and are shown in Table 1. The insulation consists of three types of graphite insulations whose properties are presented in Table 2, together with other material properties used in simulations. The right side of the simplified furnace geometry shown in Fig. 1 corresponds to the symmetry axis of the 2D axisymmetric model.

The furnace geometry was meshed in ANSYS Workbench, and the thermal simulations were run in ANSYS Fluent®. A conformal mesh with mostly square elements was generated to ensure mesh continuity at solid–fluid or solid–solid interfaces. The general mesh size is 3 mm, but some parts as sapphire, heaters and crucible have mesh sizes less than 1 mm to ensure sharp melt–crystal interface and

Table 1 Material properties of sapphire melt and crystal

Density crystal (Kg/m <sup>3</sup> )	3960
Density melt (Kg/m <sup>3</sup> )	3000
Thermal conductivity crystal (W/m K)	5,4
Thermal conductivity melt (W/m K)	3,5
Specific heat crystal (J/Kg K)	1097,5
Specific heat melt (J/Kg K)	1012,5
Melting temperature (K)	2323
Solidification heat (J/Kg)	1,407,000
Dynamic viscosity (Kg/m s)	0,0575
Latent heat of fusion (KJ/Kg)	1100
Absorption coefficient crystal (1/m)	19
Absorption coefficient melt (1/m)	1019
Refractive index crystal	1,78
Refractive crystal melt	1,78

proper energy conduction. The total number of elements is approximately 110,000. All domains are coupled to ensure temperature continuity and heat flux conservation at all interior boundaries.

#### **Process Simulation Model**

The modeling of sapphire growth in furnaces is a complex task because of a multitude of physical processes that take place in different regions of the furnace. First, there is a global heat transfer from heaters to Ar atmosphere, sapphire and different solid parts of the furnace, and because of the large temperatures needed for sapphire melting, the radiative heat flux at all solid walls in furnace cannot be neglected. Then, the sapphire is subject to different heat fluxes which determine the solidification process: In the HEM method, there is cooling at the crucible bottom and heating through the crucible lateral walls and from the atmosphere above; within the sapphire itself, the heat is transported via conduction, convection and internal radiation, where internal radiation (absorption and emission) plays an essential role. In order to highlight the main heat transfer mechanisms in different parts of the furnace, separate subsections are presented in the following, with models characteristic for each region.

The effect of various heat transfer mechanisms on the temperature distribution, melt flow field and melt-crystal interface shape during the crystal growth of sapphire was the subject of more studies [8, 9]. Some simulation models of sapphire growth use crucible sub-models with convective boundary conditions at the crucible walls to account for the heat transfer from the furnace and heat extraction from the heat exchanger [7, 14]. Here, we employ a coupled approach where the global heat transfer and the heat exchange and solidification in the sapphire are solved simultaneously. In the model used for the simulation in this publication, a constant heat flux is applied at the bottom of the crucible as the driving force of the crystallization process. The absolute value of this cooling flux is corresponding to the radiative cooling flux extracted from the furnace, and it is calculated based on the stationary calculations from the

Table 2 Material properties of different parts used in simulations

Material	Density (kg/m <sup>3</sup> )	Specific heat (J/kg K)	Thermal conductivity (W/m K)	Emissivity
Heaters (top, side)	1770	Temperature dependent	85	0.8
Molybdenum crucible	10,280	250	120	0.25
Graphite insulation 1	180	Temperature dependent	Temperature dependent (Fig. 2)	0.9
Graphite insulation 2	90	Temperature dependent	Temperature dependent (Fig. 2)	0.9
Graphite insulation 3	1500	Temperature dependent	30	0.8
Argon atmosphere	1.78	520	0.0172	



simulation setup for the original furnace. The top and side heaters are simulated as volumetric heat sources that provide energy corresponding to industrial heaters power. At the outer boundaries, the following conditions are considered: (1) A uniform cooling flux of  $-50,000 \text{ W/m}^2$  is applied at the crucible bottom, and (2) a constant temperature boundary condition (800 K) is applied on the outer walls of the graphite insulation, approximated from previous furnace simulations. Although these conditions change slightly in the technological growth process, they are kept constant in the present simulations for simplicity reasons.

#### **Global Heat Transfer in Furnace**

As previously stated, the thermal simulations of the furnace sapphire system are conducted in ANSYS Fluent®. Here, a general energy equation is solved in the fluid zones, including convection, conduction, species diffusion, viscous dissipation and other heat sources. In the furnace sapphire model considered here, there is no species diffusion, and the viscous heating can be neglected. When a radiation model is used, the radiative heat flux is used as a source term. Therefore, the energy equation in the fluid zones (Ar atmosphere, sapphire) can be written as follows:

$$\frac{\partial}{\partial t}(\rho E) + \nabla \cdot (\rho \vec{v} E) = \nabla \cdot (k_{\text{eff}} \nabla T) - \nabla \cdot \vec{q}_{\text{rad}}$$
 (1)

In the Ar atmosphere, the energy  $E = h = \int_{T_{a}}^{T} C_{p} dT$ , where h is the sensible enthalpy,  $T_{\text{ref}} = 298,15 \text{ K}$  and  $C_p$  is the fluid specific heat. In sapphire, the latent heat of solidification (L) is added: $H = h + \beta L = h_{ref} + \int_{T_{-r}}^{T} C_p dT + \beta L$ , where  $\beta$  is the sapphire liquid fraction. The convective term  $\nabla \cdot (\rho \vec{v} E)$  is relevant for the sapphire melt flow, but the convection of Ar atmosphere is neglected in the current model since the furnace is operating at low atmosphere pressure. The effective thermal conductivity  $k_{\text{eff}} = k + k_t$ , where  $k_t$  is a contribution from the turbulence, when a turbulent model is used. The radiation heat has different interpretations in sapphire compared to Ar atmosphere. While sapphire is a participating semi-transparent medium, where incoming radiation can be absorbed, emitted and scattered, the Ar atmosphere is a non-participating medium and does not interact with radiation. However, the radiation energy is absorbed and emitted at the gas-solid interfaces, and this contribution is essential in furnaces operating at high temperatures as is here the case. The radiation model and the boundary conditions used for the opaque (gas-solid) and semi-transparent (gas-melt) interfaces are presented in Sect. "Radiation model."



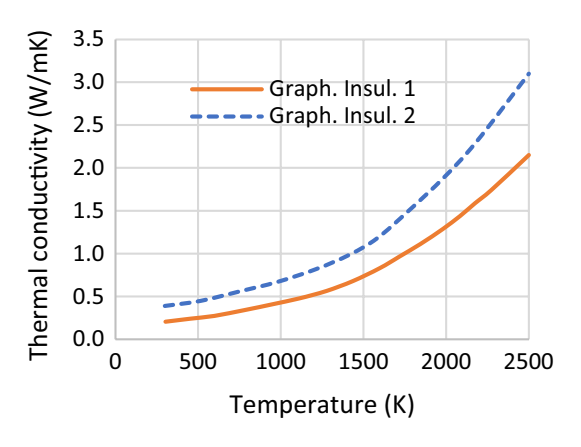


Fig. 2 Temperature-dependent thermal conductivities of graphite insulations used in simulations (available material data)

In the solid parts of the furnace, the heat is transferred only by conduction, and a source term is added in heaters to account for the heating power:

$$\rho_s \frac{d}{dt} \left( \int_{T_{ref}}^T C_p dT \right) = \nabla \cdot \left( k_s \nabla T \right) + S_{\text{heater}}$$
 (2)

Here  $\rho_s$ ,  $C_p$  and  $k_s$  correspond to each solid part of the furnace, shown in Table 2 and Fig. 2.  $S_{\text{heater}}$  is a volumetric heat source term related to the technological heater power and is implemented as volumetric heat source only in the top and side heaters ( $P_{\text{heater}}/V_{\text{heater}}$ ).

### **Radiation Model**

The general form of the radiative flux is an integral of the radiation intensity I as a function of distance  $\vec{r}$  and direction  $\vec{s}$  within the solid angle  $d\Omega$ .

$$\vec{q}_{\rm rad} = \int_{4\pi} I(\vec{r}, \vec{s}) \cdot \vec{s} d\Omega \tag{3}$$

Because of the large absorption, emission and scattering properties of sapphire crystal and melt, internal radiation plays an essential role in heat transfer during the sapphire growth. Many studies have shown that internal radiation enhances the heat transport through crystal and reduces the temperature gradient and thermal stress in the central body of the crystal, but leads to a significant increase in the temperature gradient and thermal stress in the bottom region of the crystal [9, 18, 19]. Therefore, a good modeling of internal radiation in sapphire is necessary. Discrete ordinates (DO) is one of the most developed radiation models and is used to simulate the radiative heat transfer including the participating media. The DO model is based on the radiative transport equation (RTE) (Eq. 4) which considers the rate of change of the radiation

intensity *I* as it travels through a medium and experiences absorption, emission and scattering in the medium.

$$\frac{d(I(\vec{r},\vec{s}))}{dt} + (a + \sigma_s)I(\vec{r},\vec{s}) = a\frac{n^2\sigma T^4}{\pi} + \frac{\sigma}{4\pi} \int_0^{4\pi} I(\vec{r},\vec{s'})\Phi(\vec{s},\vec{s'})d\Omega'$$
(4)

Here  $\vec{r}$  is the position vector,  $\vec{s}$  is the direction vector,  $\vec{s}'$  is the scattering direction vector, a is the absorption coefficient,  $\sigma_s$  is the scattering coefficient, n is the refractive index,  $\sigma$  is the Stefan–Boltzmann constant, T is local temperature,  $\Phi$  is phase function and  $\Omega t$  is a solid angle.

Discrete ordinates (DO) model solves the radiative transfer equation for a finite number of discrete solid angles, each associated with a direction  $\vec{s}$ , fixed in a global cartesian system (x, y, z). Thus, from an infinite number of directions, only a finite number of directions are chosen, and for each discrete direction, a radiation transport equation is solved. DO does not perform ray tracing, but solves the RTE (Eq. 4) as a transport equation, similar to energy and mass transport. DO solves as many equations as there are directions  $\vec{s}$ . Therefore, one limitation of DO method is the computational expense to solve new transport equations in addition to flow and energy equations. In view of that, the number of discrete angles should be optimally chosen. One simplification used in Fluent ANSYS is that only one octant of the total solid angle is used because of symmetry reasons, and this octant is discretized in N<sub>\infty</sub> azimuthal angles sand  $N_{\theta}$  polar angles. In the current furnace simulations, different discretization schemes were tested, and finally, the number of discretized polar and azimuthal angles was chosen as  $4 \times 4$  ( $N_{\alpha} = N_{\theta} = 4$ ). Despite the computational cost, DO is one of the few methods that can solve problems ranging from surface to surface radiation to participating media and radiation of semi-transparent walls, and from this reason, it is frequently used in the literature.

The boundary conditions of Eq. 4 depend on the wall type: Furnace internal walls that are in contact to Ar atmosphere (like insulation or steel casing) are considered opaque walls, whereas the interface between atmosphere and sapphire is treated as a specular semi-transparent wall. A complete description of different boundary conditions related to opaque or semi-transparent walls in the DO radiation model can be found in Fluent ANSYS Theory Manual, Sects. 5.3.6.6 and 5.3.6.7, respectively. For simplicity, only the boundary conditions of gray diffuse radiation at opaque walls are shown here. As stated in Sect. "Global heat transfer in furnace," the Ar atmosphere is a non-participating medium meaning that no internal radiation is dissipated/ absorbed in the atmosphere. The radiation travels back and forth between gas-solid interfaces, where it is absorbed and emitted based on the wall emissivity, temperature and the medium refractive index. For a gray diffuse radiation, the

incident radiation flux at a wall with normal vector  $\vec{n}$  is as follows:

$$q_{\rm in} = \int I_{\rm in} \vec{s} . \vec{n} d\Omega \tag{5}$$

Assuming that a fraction  $\epsilon_w q_{\rm in}$  of incident radiation is absorbed by the wall, with  $\epsilon_w$  being the wall emissivity, the net radiation flux leaving the surface is as follows:

$$q_{\text{out}} = (1 - \epsilon_w)q_{\text{in}} + n^2 \epsilon_w^2 \sigma T_w^4$$
 (6)

Where n is the medium refraction index,  $\sigma$  is the Boltzmann constant and  $T_w$  is the wall temperature. Thus, in Ar atmosphere, the DO radiation model is reduced to a surface to surface radiation model. In sapphire, however, the discretized radiative transport equations (Eq. 4) have to be solved as additional transport equations.

### **Solidification Model in Sapphire**

The solidification model implemented in ANSYS Fluent is based on the enthalpy–porosity technique. In this technique, the melt–crystal interface is not tracked explicitly, but a quantity—called liquid fraction—is defined in each cell of the domain, which tracks the fraction of the cell that is occupied by liquid. The liquid fraction ( $\beta$ ) can take values of 1 in the liquid (melt) phase, 0 in the solid (crystal) phase and an intermediate value in the transition zone between melt and solid, called mushy zone. The mushy zone is treated as a pseudo-porous medium whose porosity decreases from 1 to 0 as the material solidifies. The porosity is equal to the liquid fraction, and for cases where  $T_{\text{solidus}} = T_{\text{liquidus}}$ , a method based on specific heat given by Voller and Prakash is used [17].

Basically, the energy equation (Eq. 1) with  $E = H = h_{ref} + \int_{T_{ref}}^{T} C_p dT h_{ref} + \beta L$  is solved for temperature,

and a sapphire cell is set as melt or crystal if the temperature is above or below the melting/solidification temperature. The mushy zone between the fully crystal and melt phases consists of cells where the temperature equals the sapphire melting/solidification temperature ( $T_{\rm solidus} = T_{\rm liquidus} = 2323~{\rm K}$ ), and where the liquid fraction takes values between 0 and 1.

The sapphire properties in the transition zone are computed with a linear mixing rule based on pure solid/liquid phase properties:  $k = (1 - \beta)k_{\text{solid}} + \beta k_{\text{liquid}}$ . As an example, Fig. 3 shows the thermal conductivity in the crystal, melt and in the mushy zone at a time instant during growth.



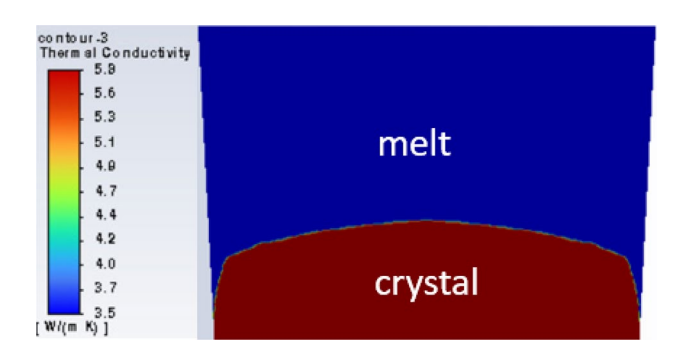


Fig. 3 Thermal conductivity in the sapphire domain: melt (blue), crystal (red) and mushy zone (yellow)

### Flow Modeling in Sapphire

The Navier–Stokes equation solved in Fluent for calculating the flow field is as follows:

$$\frac{\partial}{\partial t} (\rho \vec{v}) + \vec{v} \nabla \cdot (\rho \vec{v}) = -\nabla p + \mu \nabla^2 \cdot \vec{v} + S \tag{7}$$

Where  $\vec{v}$  is the sapphire velocity, p is the static pressure,  $\mu$  is the dynamic viscosity of sapphire melt and S is the momentum sink term that can have various sources. The terms on the left side are related to the convective transport, whereas on the right side, the volumetric stress contribution and the momentum diffusion term are included. Since sapphire undergoes a phase transformation from melt to solid and can contain domains of melt and domains of solid sapphire, a momentum sink term is added in the Navier–Stokes equation, which has the effect of reducing the velocity to zero in the crystalized zone:

$$S = \frac{(1-\beta)^2}{\beta^2 + \varepsilon} A_{\text{mush}} \vec{v} \tag{8}$$

Here  $\varepsilon$  is a small number (0.001) to prevent division by zero,  $A_{\rm mush}$  is the mushy zone constant and  $\vec{v}$  is the melt velocity. The mushy zone constant acts as a damping factor and determines the transition of the velocity of the material to zero as it solidifies; the higher this value, the steeper the transition.

Because of the furnace heating, the sapphire melt experiences a natural convection flow, and due to the low melt flow velocities (~10<sup>-4</sup> m/s), a laminar model is here used. The sapphire melt is incompressible, and the Boussinesq assumption is applied. The melt free surface is flat, and the Marangoni effect is neglected (in other simulations with Marangoni forces, it has been found that those were negligible compared to buoyant forces in the HEM setup). A flow pattern is shown in Fig. 4 at a time instant during the growth stage. The natural convection flow of the melt is emphasized: The melt moves parallel to the melt–crystal (m–c) interface outwards, then upwards parallel to the side crucible walls

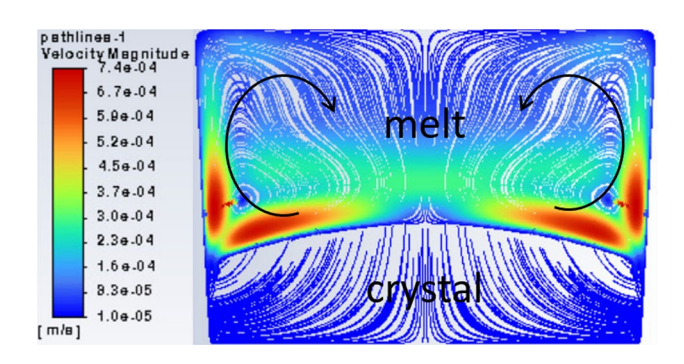


Fig. 4 Flow field in the sapphire melt at a time instant during the growth phase

and then inwards to the sapphire axis. The melt flow next to the m-c interface has the effect of flattening the crystal growth front, opposite to the effect of internal radiation in crystal as shown in [8]. Therefore, in the HEM setup, the melt convection has a beneficial effect because it reduces the m-c interface convexity and subsequently the radial stress and dislocation density.

#### **PID Control Loop for Sapphire Seed Formation**

In the HEM technological growth process, a sapphire seed is placed and kept cool on the crucible bottom while the sapphire raw material above is melted by increasing the heaters power. Since the sapphire raw material is a powder and its properties are difficult to predict exactly, a different approach to generate the sapphire seed and the corresponding temperature field at the seeding point is employed in current simulations. All sapphire material is considered initially either melted or solidified, and the top heater power is adjusted by a PID control loop to obtain a temperature equal to the solidification/melting temperature at the top seed position. The implemented controller equation of the top heater power is as follows [20]:

$$u(t) = K_p \left[ e(t) + \frac{1}{T_n} \int_0^t e(t) dt + T_v \frac{de(t)}{dt} \right]$$
 (9)

Where u(t) represents the top heater power,  $e(t) = T_{\rm controlpoint} - T_{\rm desired}$  is the deviation of the control temperature at the top seed position from the desired temperature (i.e., the solidification temperature),  $K_p$  is the proportional term and  $T_n$  and  $T_v$  are related to integral, respectively, differential terms of the control equation. The differential term has the effect of damping big fluctuations due to overshooting of the proportional term, whereas the integral term ensures better convergence to the desired value. The proportional, differential and integral coefficients are varied until a smooth convergence to the desired temperature is reached.



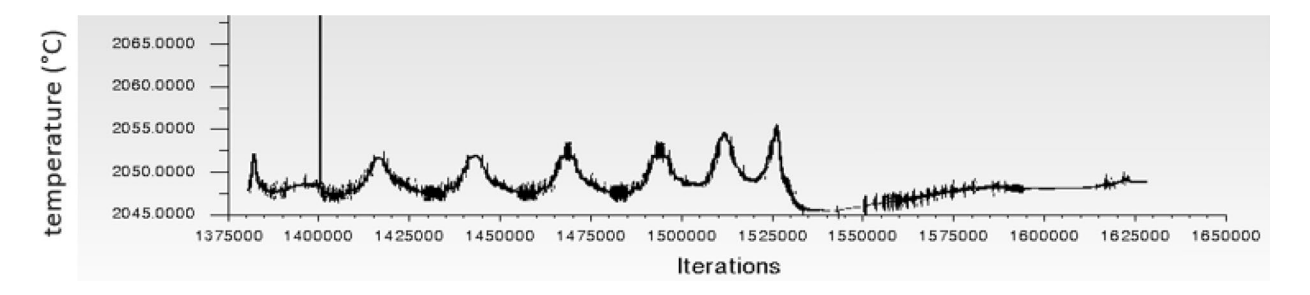


Fig. 5 The variation of the control temperature (at the seed height position) during the PID seed simulation

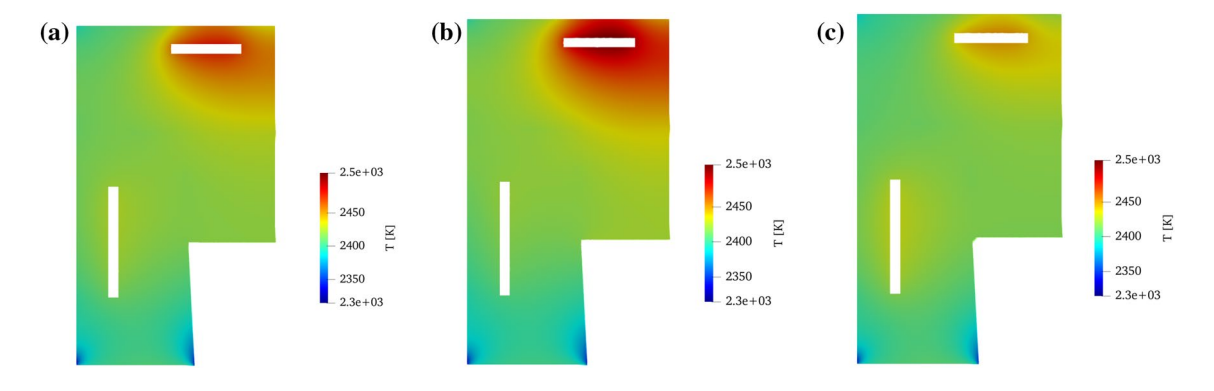


Fig. 6 Temperature field in the atmosphere at the seeding point: **a** Case 1:  $T_{top\ heater} = 2471\ K$  and  $T_{side\ heater} = 2422\ K$ , **b** Case 2:  $T_{top\ heater} = 2496\ K$  and  $T_{side\ heater} = 2416\ K$ , and **c** Case 3:  $T_{top\ heater} = 2450\ K$  and  $T_{side\ heater} = 2428\ K$ . The same scale range is used for all cases

The PID control loop is not available in Fluent ANSYS, but is developed in-house and implemented as a user-defined function in Fluent simulations. The top heater power is adapted, and the side heater heat source is kept constant. The temperature at the top seed position is monitored so that it converges to the melting/solidification temperature of sapphire. Figure 5 shows the monitoring of the top seed temperature during the steady PID loop simulation. Here, the proportional, differential and integral coefficients were varied in a first stage until the optimal parameters were found, and a smooth convergence to the melting/solidification temperature (2050 °C) was reached. Because the top heater is relatively far away from the sapphire seed that is placed on the crucible bottom, the PID control loop simulation is in this case challenging, and many iterations are needed to reach a constant top heater power for the desired top seed temperature. However, by carefully varying the proportional, differential and integral coefficients in the PID simulation, a stable top heater power can be found for a stable seed formation of dimensions similar to the sapphire seed in the technological process.

#### **Results and Discussion**

## Seed Formation for Different Top and Side Power Distributions

The PID method described above was used for three cases with different top and side power distributions, but same total power. In Case 1, the top and side heater power have similar magnitudes:  $P_{\text{top}} = 12.9 \text{ kW}$  and  $P_{\text{side}} = 13.6 \text{ kW}$ ; in Case 2, the top heater power is twice the side heater power:  $P_{\text{top}} = 17.67 \text{ kW}$  and  $P_{\text{side}} = 8.83 \text{ kW}$  and, in Case 3, the top heater power is half the side heater power:  $P_{\text{top}} = 8.83 \text{ kW}$  and  $P_{\text{side}} = 17.67 \text{ kW}$ . In simulations, the volumetric heat sources are used instead of heaters power. The volumetric heat source is defined as P/V, where P is the heater power, and V is the volume of the respective heater. The top heater volume is  $0.0006 \text{ m}^3$  and the side heater volume =  $0.0022 \text{ m}^3$ .

In all cases studied here, only the top heater power was adapted in the PID control loop, and the side heater power was fixed. In each case, a PID steady simulation was conducted until the temperature at the top seed position converged to the sapphire melting/solidification temperature. The other process parameters, crucible cooling heat flux  $(-50,000 \text{ W/m}^2)$  and the insulation outer temperature



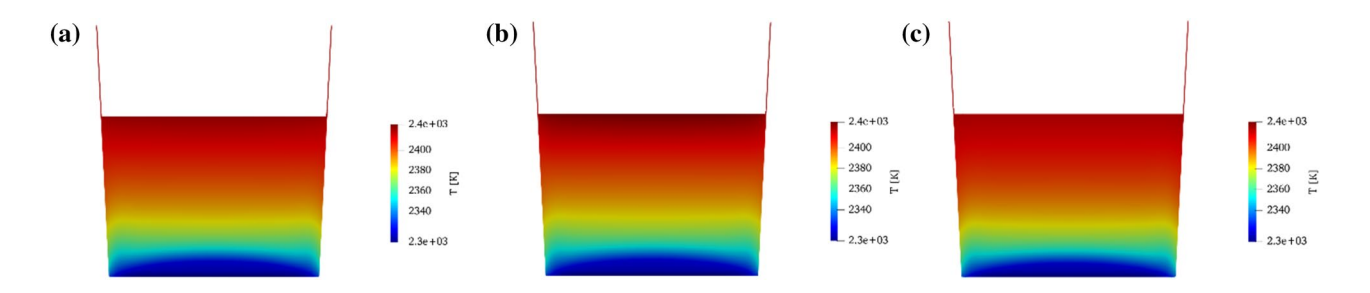


Fig. 7 Temperature field in sapphire and crucible at the seeding point: **a** Case 1, **b** Case 2, and **c** Case 3. The maximum temperature in sapphire is found on the top surface: **a** 2419 K, **b** 2424 K, and **c** 2417 K. The temperature at the sapphire bottom (Symmetry axis) is 2310 K in all cases

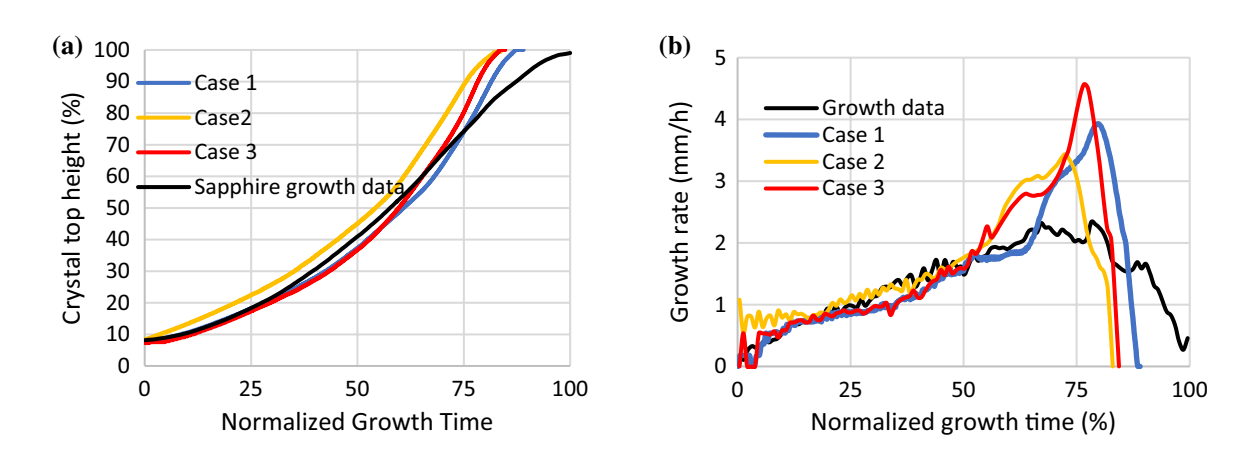


Fig. 8 Evolution of sapphire crystal height (a) and growth rate (b) during the growth stage. The crystal height and the growth time are scaled to the maximum crystal height and the maximum growth time (technological growth time), respectively

(800 K), are the same in all cases. In Fig. 6, the temperature fields in atmosphere for Cases 1, 2 and 3 are shown. Because of the different top and side heater power ratio, the global thermal fields look different especially around the heaters. However, next to the crucible wall, the temperature field is more homogeneous, and differences are indistinguishable. This can be better seen in Fig. 7, which shows the temperature field in sapphire and crucible at the seeding point. The local thermal conditions next to the crucible bottom are similar in all cases at the seeding point, being determined by the cooling flux at the crucible bottom which is the same in all cases. Only close to the top sapphire surface, different temperature magnitudes are found and can be related to different heater power distributions, i.e., highest temperature at the sapphire top in Case 2 and lowest temperature at the sapphire top in Case 3 as shown in figure captions.

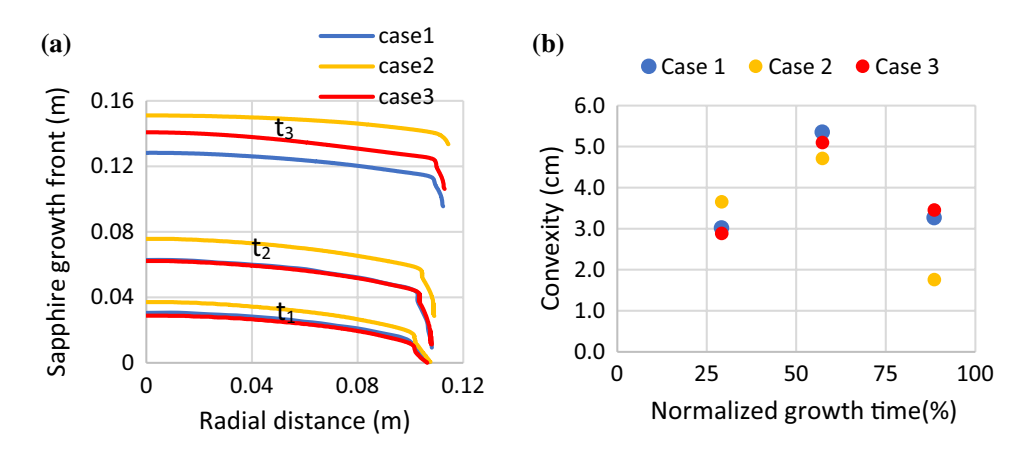
# Sapphire Growth Simulations with Heater Power Ramp-Down

Sapphire growth settings used in the present simulations rely on a technological growth process, where the top heater power is ramped down, and the side heater power is kept constant. The ramp-down rate of power is 0,00806 W/s; therefore, the top heater power decreases in time as  $P_{\text{top, seeding}}$ —0,00806 (W/s) \* time(s) and  $P_{\text{side}} = P_{\text{side, seeding}} = \text{constant}$ . The same ramp-down power rate is used in all three cases, and although different initial top and side heater powers are considered in each case, the total power is the same. Therefore, the total energy decreases by the same rate in all cases, with a different temperature distribution in furnace in each case. The values of the initial top and side powers at the seeding point for three cases were given in the previous section. The cooling flux at the crucible bottom (-50,000 W/m<sup>2</sup>) and the outer insulation temperature (800 K) are assumed to stay constant during the growth period in simulations. This assumption is based on the fact that in the real technological process, these conditions change only slightly during the growth stage, and this change is not expected to affect qualitatively the results of this study.

Transient computations were conducted for each case to simulate the sapphire crystal growth. Figure 8 shows the results of the simulated crystal growth in each case and interface position tracking data from an industrial sapphire crystal growth process: (a) maximum crystal height and (b)



Fig. 9 a Sapphire growth front at various growth times for Case 1:  $P_{\text{top}} \sim P_{\text{side}}$ , Case 2:  $P_{\text{top}} = 2P_{\text{side}}$  and Case 3:  $P_{\text{top}} = P_{\text{side}}/2$ . b m—c interface convexity corresponding to time steps in (a); the growth time is normalized to the total growth time of Case 1.



the growth rate during the growth stage. The differences between the simulated and the measured data can be attributed to various factors: (1) Different power magnitudes are used in the technological and simulated processes, and (2) simplified furnace geometry and boundary conditions used in simulations. However, the intention of the current simulations was not to reproduce the measured data, but to create realistic cases where the sapphire crystal grows in a similar way to an industrial growth process. As noticed in Fig. 8, the overall growth behavior is similar: 1) The evolution of sapphire crystal height and growth rate in time is the same order of magnitude as the technological data, and 2) the crystal height vs. time has an S-shape both in measurement and in simulations. In the first half of the growth stage, the crystal height and growth rate are similar in all cases and are in good agreement with the technological process. This can be explained by the fact that in this growth phase, the similar cooling fluxes at the crucible bottom and the ramp-down rates have the biggest impact on crystal growth, both in simulation as well as in the technological processes. Case 2  $(P_{top} = 2P_{side})$  which corresponds to lowest side heater power exhibits a slightly higher growth rate at growth begin than Cases 1 ( $P_{\text{top}} \sim 2P_{\text{side}}$ ) and 3 ( $P_{\text{top}} = P_{\text{side}}/2$ ), because of the colder side thermal environment. However, it is seen that different heater power ratios do not affect the growth rate in the first half of the growth stage. The growth rate differs mostly in the second half of the growth stage, indicating the influence of the different heaters power distribution. The maximum growth rate is obtained for Case 3 which corresponds to the largest radial to axial heat flux ratio. A more detailed analysis of the main contributing factors during the growth stage is presented in the next section.

# Comparison of the Melt–Crystal Interface for Different Heater Power Distributions

As mentioned in introduction, the sapphire m—c interface shape is related to the quality of the crystal growth process,

since interfaces with large convexities can promote the formation of facets with different orientations and, therefore, lead to low angle grain boundary defects [1]. Various studies have been performed to reduce the sapphire m-c interface convexity, where convexity is defined as the difference between the maximum and minimum height of the m-c interface at a time instant. For example, in the classical HEM with He cooling, the diameter of the cooling system can be optimized to reduce the obtuse angle of the m-c interface and eliminate the hot spots that appear at the crucible corners [7]. Other studies have shown that by modifying the geometry of the supporting cooling system, the radial and axial heat flow in sapphire can be optimized so that a flatter m-c interface can be obtained [8]. The idea of radial to axial heat transfer ratio  $(Q_a/Q_a)$  can be also exploited by moving the crucible in relation to the side heater and by selecting the position where  $Q_r/Q_a$  is minimum, which corresponds to lowest interface convexity [13]. In the present study, we do not make any geometrical changes to the furnace geometry, but use only different top and side heater power ratios to investigate the influence of different power arrangements on the thermal field and on the m-c interface shape. The cooling mechanism at the crucible bottom is considered only in terms of a cooling heat flux extracted from the furnace, as described in Sect. "Process simulation model."

As shown in the previous section, the sapphire crystal height and growth rate in the first part of the growth phase are not affected by the different distributions of top and side heater energies. How about the shape of the melt–crystal interface? It is expected that the local thermal field at different crucible positions is different for various top and side heater power values, because higher side power results in larger radial thermal gradient and interface convexity. In this respect, the m–c interface shape was monitored during the growth simulation in each case. Figure 9 shows the interface shapes (a) and the interface convexity values (b) at three time instants: at the beginning  $(t_1)$ , in the middle  $(t_2)$  and close to the end of the growth phase  $(t_3)$ . As can be noticed,



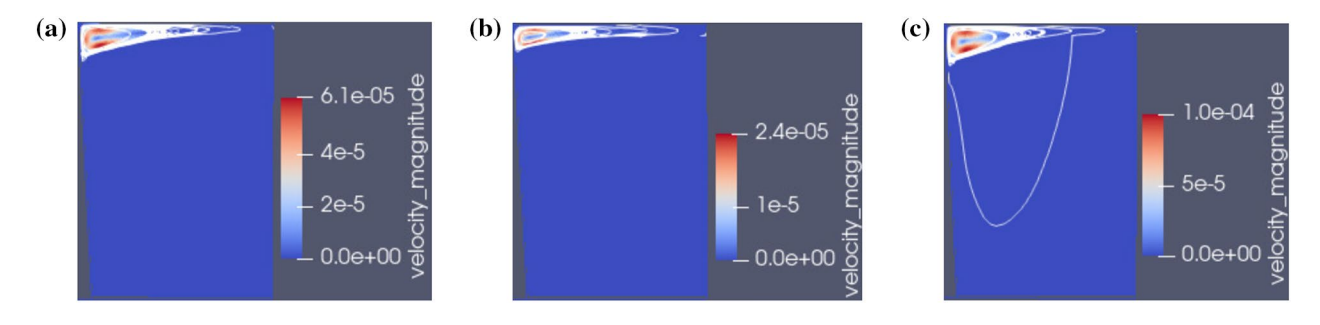


Fig. 10 Sapphire melt flow streamlines at the end of the growth phase for: a Case 1, b Case 2, and c Case 3

the convexity values of all cases increase toward the middle of the growth  $(t_2)$  and decrease again at the end of the growth phase  $(t_3)$ . At time instant  $t_1$ , the height and the convexity of Case 2 ( $P_{\text{top}} = 2 \times P_{\text{side}}$ ) are somewhat larger than for Cases 1 and 3, because of the coldest environment at the lower crucible side. However, the differences are very small, meaning that the cooling flux at the crucible bottom is dominant in this time interval, whereas the top/side power distribution is negligible. A similar behavior can be observed at  $t_2$ , but with an increased convexity close to the crucible walls indicative of a stronger radial heat flow and higher radial thermal gradients. After the interface convexity increases in the first half of the growth stage, it decreases again toward the end of the growth stage as shown in Fig. 9 at  $t_3$ . Here, a clear influence of the local thermal field can be noticed: The growth front shape of Case 2 is flatter, because the weaker side heating and the stronger top heating energies produce a smaller radial to axial heat flux ratio compared to the other cases. The buoyant flow of the melt is induced by the side and top heating, but the heat coming through the crucible lateral walls is essential. A stronger side heating results in a stronger convection close to crucible as shown in Fig. 10, where a comparison of the melt flow streamlines at the end of the growth stage for similar crystal height is presented. As can be noticed, the flow streamlines in Cases 1 (a) and 3 (c) are concentrated closer to the side crucible wall whereas the streamlines in Case 2 are flatter and parallel to the sapphire free surface. A lower convexity is beneficial for growing sapphires with low density of surface dislocations, but other factors, such as growth rate and axial temperature gradients, are also relevant in the formation of dislocations.

# Application of the Crystal Plasticity Model to Sapphire Growth Process

As mentioned earlier, the generation of defects, such as dislocations, occurs frequently in the sapphire growth applications, and one of the decisive parameters influencing the generation of defects is the crystal growth rate and the convexity of the growth surface. In this section, a dislocation-based crystal plasticity finite element (CPFEM) model is applied to evaluate the effect of the growth surface convexity on the generation of dislocations. The crystal plasticity (CP) model is implemented into the FEM software of ABAQUS through an open-source Fortran subroutine, so called CP-DAMASK toolbox. The CP model and its mathematical descriptions are not presented here, but readers are referred to, e.g. [15, 21], for details about this material model. For the use of crystal plasticity model, it is first necessary to determine the constitutive parameters; obtaining these parameters usually requires a wide range of FEM simulations. The CP material parameters have been derived for sapphire crystal from the experimental strain-stress curves. The stress-displacement curves of sapphire, obtained from the tensile tests conducted on single-crystal rods, at different temperatures and strain rate  $(\dot{\varepsilon})$  values, are available from the literature [22]. The stress-strain response of crystalline sapphire has been simulated for different temperatures and strain rate values, and the all CP parameters have been determined by fitting the simulation and the experimental curves. A temperatureand strain rate-dependent thermally-activated constitutive law has been developed for the correct estimation of dislocation velocity and plastic flow at different temperatures and  $\dot{\varepsilon}$ -values. The derivation of CP parameters is not included in this paper, as it requires a separate paper to fully cover all details. For details, see our future paper [23] (in preparation for publication).



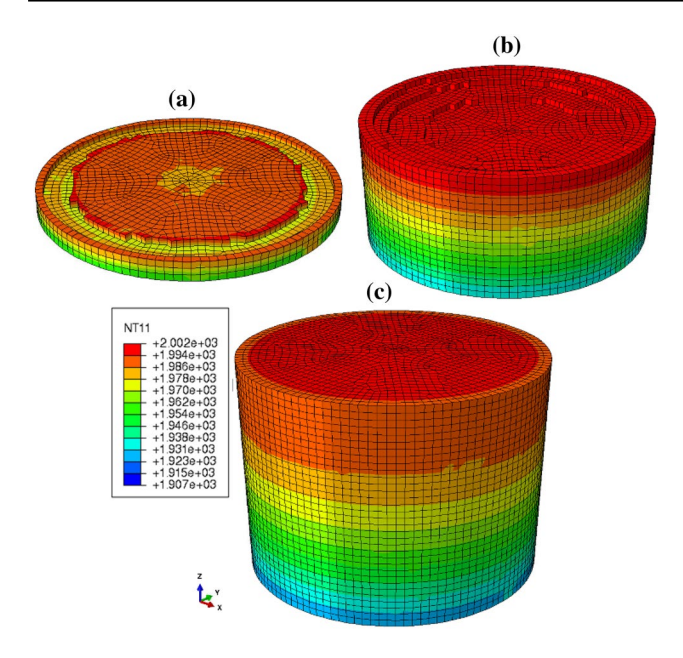


Fig. 11 Temperature distribution in the concave growth shape at different growth times,  $\bf a$  at the beginning,  $\bf b$  at the middle, and  $\bf c$  at the end of growth

By the combination of ABAQUS and DAMASK, the crystal deformation and dislocation density evolutions are simulated during the growth stage. The simulation of the crystal growth stage consists of three steps. In the first step, the crystal growth is modeled by the 2D axisymmetric CFD

computations (with ANSYS FLUENT), as explained in the previous sections. In the second step, temperature and liquid fraction data of each FEM node are extracted from the 2D CFD simulations at various growth times, and then, the data are transformed into 3D by self-written scripts. In the third step, the 3D thermo-mechanical simulations (using static/implicit time integration) are performed by ABAQUS. With the liquid fraction data provided vs. time, the crystal growth process is stimulated by the model—change interaction module of ABAQUS, where the solidification is modeled by adding elements and the liquification by removing elements, see e.g., Abaqus User Manual 2018. Figure 11 shows the growth process simulation for three different growth times with maps of temperature distribution.

The dislocation densities are evaluated by the CPFEM simulations during the growth process for two different shapes of the growth surface, a slight concave shape (see Fig. 11) and a convex shape (see Fig. 9). The convex growth interface is similar to the Case 2 presented in the Sect. "Sapphire growth simulations with heater power ramp-down," while the concave growth interface can be achieved by a different setting of the power of top and side heaters. The normalized values (normalized by the initial dislocation density value) of dislocation densities at the end of growth stage for the convex and concave shapes are presented in Figs. 12 and 13, respectively. The absolute values are not presented here because of confidentiality-related aspects. Figures 12a and 13a demonstrate the distribution of the dislocation density

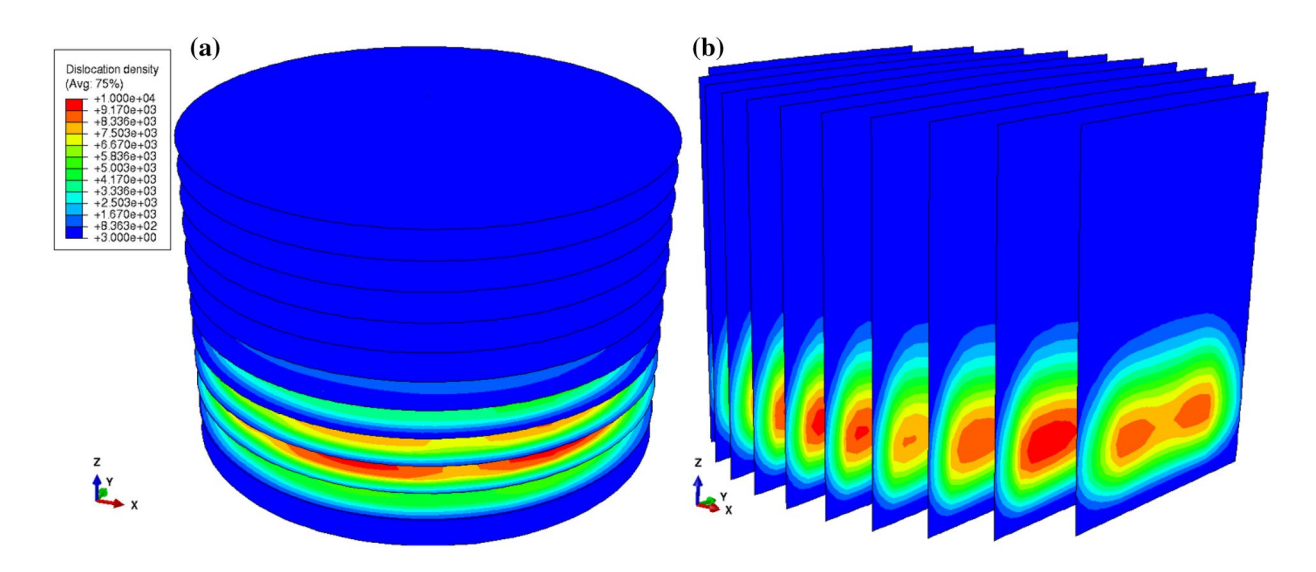


Fig. 12 The normalized basal plane dislocation density distribution in the convex shape of growth interface at the end of growth stage. **a** Dislocation distribution in a series of slices from the bottom to the top of crystal. **b** Dislocation distribution in a series of slices in the radial direction

<sup>&</sup>lt;sup>1</sup> It shall be noted that a concave interface shape might not be practical in industrial applications because of some crystallographic problems such as the formation of low angle grain boundaries.



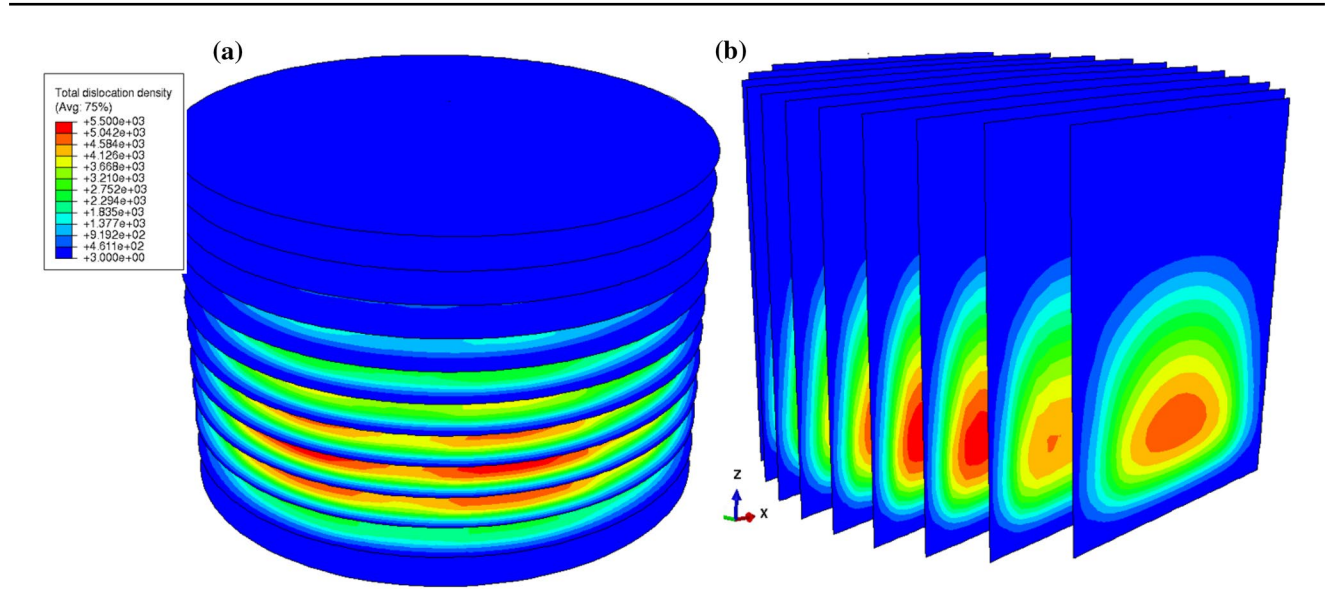


Fig. 13 The normalized basal plane dislocation density distribution in the concave shape of growth interface at the end of growth stage. a Dislocation distribution in a series of slices from the bottom to the top of crystal. b Dislocation distribution in a series of slices in the radial direction

inside the boule by a series of cuts along the z-axis (12 slices from the bottom to the top of crystal). In order to clearly detect the dislocation density distribution inside the crystal, 12 slices along the x-axis (in the radial direction) are also shown in Figs. 12b and 13b. As one can see, dislocations are mainly generated at the bottom of the boule. The maximum dislocation densities appear at distances of 30 mm (for the convex case) and 40 mm (for the concave case) from the bottom surface. The maximum value of the dislocation density for the convex case is two times higher than that of concave case. By a comparison between the dislocation density values in Figs. 12 and 13, it can be concluded that the dislocation density for a single-crystal sapphire with a concave growth interface is much lower than that for the case with a convex growth interface. The reason behind is that the temperature gradient is much larger for the convex case considered here compared to the concave case, and this causes that large difference between the dislocation density values in the crystals with the convex and concave growth interfaces.

### **Conclusions**

In this work, a 2D axisymmetric model of a simplified furnace geometry is presented, and a process simulation model tool for a sapphire growth application is introduced. The sapphire seed formation is done by using a PID control module implemented in Fluent ANSYS via an in-house developed user-defined function. Three cases with different top and side heater power ratio, but same total power, are investigated. Transient growth simulations for each case are conducted

by ramping down the top heater power at a rate similar to the experimental data. The cooling at the crucible bottom and the temperatures of the insulation outer walls are kept constant and are based on previous modified HEM calculations. In all cases, the simulated crystal growth profile and the growth rate are similar to the industrial application, indicating realistic simulation conditions. The sapphire m—c interface is monitored during the growth simulation in each case, and the interface shapes at similar growth times are compared.

In general, one can conclude that in the first part of the growth stage, the sapphire m-c interface shape is similar in all cases irrespective of different top and side power distributions. This means that the cooling mechanism and the heat transferred through the crucible walls are the main factors that influence the sapphire m-c interface shape in this growth phase. Only toward the end of the growth stage, different top and side power distributions induce different m-c interface shapes. In this last growth phase, higher top heater power causes more axial heat flow and a flatter m-c interface shape, whereas the cases with higher side heater power exhibit a higher interface convexity next to crucible walls. However, these conclusions have to be restrained to the current settings used in simulations: Same crucible cooling flux and same outer insulation wall temperatures were used in all cases. In some modified HEM growth applications, these parameters are not independent of the top and side heater powers but are intercorrelated; therefore, the boundary conditions used in our study may not apply in other HEM setups. Nevertheless, the cases shown here deliver qualitative results related to



the influence of different heater power distribution on the m-c interface shape.

By the application of the dislocation density-based crystal plasticity model, it is shown that the growth interface shape plays an important role in the generation of dislocations during the crystal growth. The CPFEM simulations demonstrate that a slight concave shape of the growth surface is beneficial for reducing grown-in dislocations. It is worth to mention that a further reduction in the dislocation densities can be achieved by optimizing the furnace structure and operation conditions, which is the focus of our future work.

**Acknowledgements** This project receives funding from FAMETEC GmbH and the Austrian Research Promotion Agency FFG.

#### **Declarations**

Conflict of interest On behalf of all authors, the corresponding author states that there is no conflict of interest.

#### References

- Bruni F (2015) Crystal growth of sapphire for substrates for highbrightness, light emitting diodes. Crys Res Technol 50(1):133–142
- Bruni F (2013) Will Czochralski growth of sapphire once again prevail? Acta Phys Polon A 124:213–218
- Xu C (2007) Thermal stresses and cracks during the growth of large-sized sapphire with SAPMAC method. Chin J Aeron 20:475–480
- Kurlov V (2016) Sapphire: properties, growth and applications: In: Materials science and materials engineering. Oxford, Elsevier, pp 1–11
- Demina S (2008) Use of numerical simulation for growing highquality sapphire crystals by the Kyropoulos method. J Crys Growth 310:1443–1447
- Ma W (2014) Numerical study of heat transfer during sapphire crystal growth by heat exchanger method. Int J Heat Mass Transf 72:425–460
- Lu C-W (2001) Numerical computation of sapphire crystal growth using heat exchanger method. J Crys Growth 225:274–281
- Zhang N (2013) Simulation of heat transfer and convection during sapphire crystal growth. J Crys Growth 367:27–34
- Ma W (2017) Role of internal radiation in oxyde crystal growth by heat exchanger method. Crystals 7:18
- Fang H (2013) Role of internal radiation at the different growth stages of sapphire by Kyropoulos method. Int J Heat Mass Trans 67:967–973
- Yu QH (2012) Local design of the hot-zone in an industrial seeded directional solidification furnace for quasi-single crystalline silicon ingots. J Crys Growth 358:5–11

- Chengai X (2007) Thermal stresses and cracks during the growth of large-sized sapphire with SAPMAC method. Chin J Aeron 20:475–480
- Wu M (2016) Effect of crucible location on heat transfer in sapphire crystal growth by Heat Exchanger Method. Heat Transf Eng 37(3–4):332–340
- Chen J (2004) Influence of the crucible geometry on the shape of the melt-crystal interface during growth of sapphire crystal using heat exchanger method. J Crys Growth 266:239–245
- Ma A, Roters F, Raabe D (2006) A dislocation density based constitutive model for crystal plasticity FEM including geometrically necessary dislocations. Acta Mater 54(8):2169–2179
- Lu P (2007) 3D simulation of the effects of growth parameters on the growth of sapphire crystals using heat exchanger method. Crys Res Technol 42:1259–1265
- Voller V (1987) A fixed-grid numerical modeling methodology for convection-diffusion mushy region phase-change problems. Int J Heat Mass Transf 30:1709–1720
- Qi X (2021) "Effect of internal radiation on heat transfer during ti:sapphire crystal growth process by heat exchanger method. Int J Heat Mass Transf 170:121000
- Ma W (2017) Investigation of heat transfer and thermal stress during sapphire crystal. J Crys Growth 468:909–913
- Chien (1952) https://de.wikipedia.org/wiki/Faustformelverfahren\_ (Automatisierungstechnik), [Online]
- 21. Roters F, Diehl M, Shanthraj P, Eisenlohr P, Reuber C, Wong SL, Maiti T, Ebrahimi A, Hochrainer T, Fabritius H-O (2019) DAMASK-the Düsseldorf advanced material simulation kit for modeling multi-physics crystal plasticity, thermal, and damage phenomena from the single crystal up to the component scale. Comput Mater Sci 158:420–478
- Kronberg M (1962) Dynamical flow properties of single crystals of sapphire, I. J Am Ceram Soc 45(6):274–279
- Sistaninia M, et al. (2024) Determination of the constitutive parameters of temperature and strain-rate dependent dislocation-density-based crystal plasticity model for single-crystalline sapphire
- Gottstein G (2004) Physical foundations of materials science.
   Springer, Berlin
- Dobrovinskaya ER, Lytvynov LA, Pishchik V (2009) Properties of sapphire. Sapphire: material, manufacturing, applications. Springer, Boston, pp 55–176

**Publisher's Note** Springer Nature remains neutral with regard to jurisdictional claims in published maps and institutional affiliations.

Springer Nature or its licensor (e.g. a society or other partner) holds exclusive rights to this article under a publishing agreement with the author(s) or other rightsholder(s); author self-archiving of the accepted manuscript version of this article is solely governed by the terms of such publishing agreement and applicable law.

